ELSEVIER

International Journal of Thermal Sciences 41 (2002) 763–772

International Journal of Thermal Sciences

www.elsevier.com/locate/ijts

A robust and accurate algorithm of the β-pdf integration and its application to turbulent methane–air diffusion combustion in a gas turbine combustor simulator

F. Liu [a,*], H. Guo [a], G.J. Smallwood [a], Ö.L. Gülder [a], M.D. Matovic [b]

[a] *Combustion Research Group, Institute for Chemical Process and Environmental Technology, National Research Council Canada, Montreal Road, Ottawa, ON, Canada, K1A 0R6*

[b] *Institute for Aerospace Studies, University of Toronto, 4925 Dufferin Street, Toronto, ON, Canada, M3H 5T6*

Received 6 February 2001; accepted 17 September 2001

Abstract

The β-pdf has been widely assumed for the probability distribution of the mixture fraction in many turbulent mixing and turbulent non-premixed combustion models in the literature. The numerical integration of the β-pdf often encounters the singularity difficulties and only few publications have addressed this issue. An efficient, accurate and robust numerical treatment of the β-pdf integration was proposed. The present treatment of the β-pdf integration was implemented into a flamelet model to calculate turbulent methane–air combustion in a model gas turbine combustor. Numerical results obtained using the present β-pdf integration method and those based on the properties of the beta and gamma functions were compared to illustrate the accuracy of the present method. Effect of assuming the β-pdf to the mass-weighted pdf and unweighted pdf of the mixture fraction on the calculated density field was also investigated.

1. Introduction

The β-pdf has been widely assumed for the probability density function of the mixture fraction in many turbulent mixing and turbulent non-premixed combustion models, see Refs. [1,2] and references cited therein. Among the turbulent non-premixed combustion models developed in the literature, the flamelet model [1] is attractive for turbulent combustion modeling due to the decoupling of flow field and chemical kinetics calculations. Because of this feature of the flamelet model, detailed chemistry mechanisms can be used in the construction of the flamelet library. In this model, only the mean density calculated using the flamelet library and the assumed β-pdf is required by the flow solver. Subsequently, species fields are calculated in a postprocessing fashion. Therefore, the numerical integration of the density field using the β-pdf should be accurate and efficient. The β-pdf consists of two parameters a and b and is written as

$$p(f) = \frac{f^{a-1}(1-f)^{b-1}}{\int_0^1 f^{a-1}(1-f)^{b-1}\,\mathrm{d}f} \tag{1}$$

The numerical integration of the β-pdf encounters difficulties due to the singularity problem at either the oxidizer side ($f = 0$) or the fuel side ($f = 1$), depending on the β-pdf parameters, and the overflow problem when the pdf parameters are sufficiently large.

Chen et al. [2], Lentini [3,4] and Lentini and Jones [5] have recently made attempts to address these issues and proposed their own treatments of the density integration assuming a β-pdf for Favre or mass-weighted pdf for the mixture fraction. The work of Chen et al. [2] contained incorrect approximations for the $a < 1$, $a < b$ and $a > b$, $b < 1$ cases. In addition, their treatment for the prevention of overflow when $a > 1$, $b > 1$ and a or b is sufficiently large is also inadequate. On the other hand, the work of Lentini [4] relies on the premise that the flamelet density distribution can be fitted to a specified functional form so that the relationships between beta and gamma functions can be used to calculate the integrations involved in the mean

* Correspondence and reprints.
E-mail address: fengshan.liu@nrc.ca (F. Liu).

1290-0729/02/$ – see front matter
PII: S1290-0729(02)01370-4

Nomenclature

a	β-pdf parameter, Eq. (1)
b	β-pdf parameter, Eq. (1)
c	polynomial coefficients, Eq. (13)
d	fitting coefficients, Eq. (15)
C_1	k–ε turbulence model parameter, Eq. (31)
C_2	k–ε turbulence model parameter, Eq. (31)
C_μ	k–ε turbulence model parameter
C_{g1}	g-equation parameter, Eq. (33)
C_{g2}	g-equation parameter, Eq. (33)
f	mixture fraction
g	variance of the mixture fraction
G	production rate of turbulence kinetic energy
k	turbulence kinetic energy
p	pressure, probability density function
r	radial position
u	axial velocity
v	radial velocity
x	coordinates

Greek symbols

ε	dissipation rate of turbulence kinetic energy; a small parameter defined in Eq. (18)
ρ	density
σ_k	k–ε turbulence model parameter, Eq. (30)
σ_ε	k–ε turbulence model parameter, Eq. (31)
σ_f	f-equation parameter, Eq. (32)
σ_g	g-equation parameter, Eq. (33)
μ_t	turbulence viscosity

Subscript

fuel	fuel
max	maximum
ox	oxidizer
ref	reference

density calculation. However, this approach is in general not applicable to mean species calculations or situations where the flamelet density distribution cannot be fitted to the specified function. The approach proposed by Lentini has been employed recently by Kumar and Tamaru [6].

In this study, a robust and accurate treatment of the β-pdf density integration was proposed. The method suggested here can also be easily extended to any other thermochemical scalars. It was implemented into a 3D finite-volume code to calculate turbulent non-premixed methane-air combustion in a model gas turbine combustor. The β-pdf integration approach of Lentini [4] was also used in the present study. Results based on the present β-pdf integration and the method of Lentini were compared. Effects of assuming the β-pdf to the mass-weighted and unweighted pdf of the mixture fraction on the results were also investigated.

2. Formulation

The Favre or mass-weighted β-pdf is written as (symbols with tilde denote mass-averaged quantities)

$$\tilde{p}(f) = \frac{f^{a-1}(1-f)^{b-1}}{\int_0^1 f^{a-1}(1-f)^{b-1}\,\mathrm{d}f} \tag{2}$$

where a and b are two non-negative parameters and are related to the mean and the variance of the mixture fraction, calculated by the flow solver, through

$$\tilde{f} = \int_0^1 f\,\tilde{p}(f)\,\mathrm{d}f \tag{3}$$

$$\tilde{g} = \int_0^1 \left(f-\tilde{f}\right)^2 \tilde{p}(f)\,\mathrm{d}f \tag{4}$$

It can be shown that

$$a = \tilde{f}\left[\frac{\tilde{f}(1-\tilde{f})}{\tilde{g}} - 1\right] \tag{5}$$

$$b = \left(1-\tilde{f}\right)\left[\frac{\tilde{f}(1-\tilde{f})}{\tilde{g}} - 1\right] \tag{6}$$

Before proceeding further in the presentation of the β-pdf integration, some discussions are first given about the relations between the values of a and b and the mixture fraction and its variance. The values of parameters a and b as functions of f and g, given in Eqs. (5) and (6), are plotted in Fig. 1. It can be seen that these parameters vary drastically from very small values near the boundary of the positivity requirement of a and b, i.e., $\tilde{g} \leqslant \tilde{f}(1-\tilde{f})$, to very large values as g approaches zero, especially for intermediate values of f around 0.5. The thickened solid lines in Fig. 1(a) and (b) represent the contours of $a = 1$ and $b = 1$, respectively. The contour of $a = 1$ is plotted again in Fig. 1(b) as a dashed line for the reason given below. It can be shown that the variances on contours of $a = 1$ and $b = 1$ peak at $f = 0.382$ and $f = 0.618$, respectively. The corresponding value of the variance on the contours at these two mixture fractions is 0.09. Four regions can be identified in terms of the values of a and b compared to unity, as indicated in Fig. 1(b): (I) $a < 1$, $b < 1$, (II) $a < 1$, $b > 1$, (III) $a > 1$, $b > 1$, and (IV) $a > 1$, $b < 1$. The corresponding shapes of the β-pdf in these four regions are schematically plotted in Fig. 2. The pdfs in region I have two singularities (where the value of the pdf approaches infinity), one occurs at the oxidizer side ($f \to 0$) and the other at the fuel side ($f \to 1$), and represent situations where the variance of the mixture fraction is large as a result of strong fluctuations in the mixture fraction. This type of pdf can occur anywhere in the flow field since the mixture fraction in this region varies

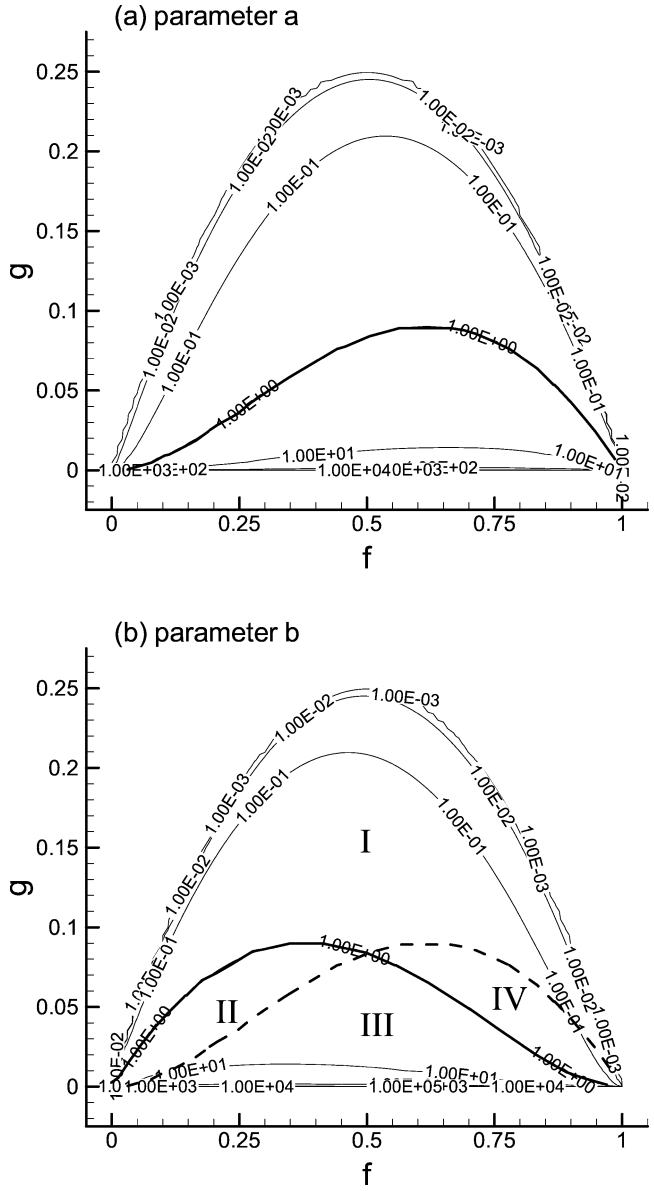

Fig. 1. Variations of parameters a and b as functions of f and g. The two contours $a = 1$ and $b = 1$ divide the $f-g$ plane into four regions: (I) $a < 1$, $b < 1$, (II) $a < 1$, $b > 1$, (III) $a > 1$, $b > 1$, and (IV) $a > 1$, $b < 1$.

from 0 to 1. The pdfs in region II have only one singularity at the oxidizer side and decays rapidly towards the fuel side. Such type of pdf represents situations of relatively large variances and relatively low mixture fractions and occurs only when the mean mixture fractions are less than 0.5, Fig. 1(b). In region III, the pdfs have no singularities and can peak at a value anywhere between 0 and 1, Fig. 2, and represent situations of relatively small variance of the mixture fraction, i.e., relatively weak fluctuations of the mixture fraction. Again, the pdfs in region III can occur anywhere in the flow field. And lastly, the pdfs in region IV are singular only at the fuel side ($f \to 1$) and decay rapidly towards the oxidizer side, Fig. 2. Such pdfs occur only at

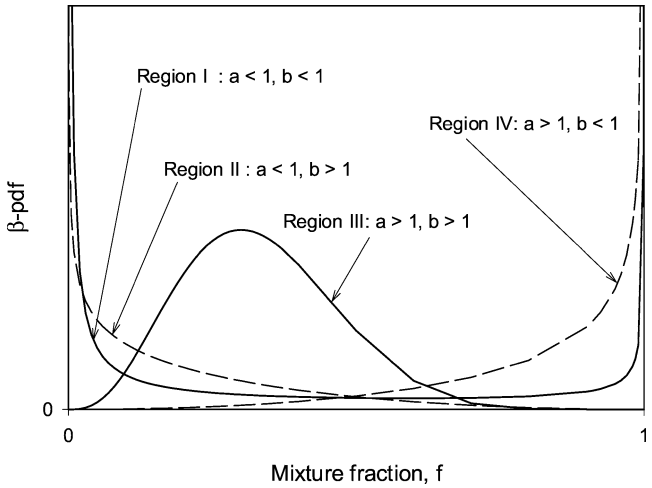

Fig. 2. Representative shapes of the β-pdf with parameters a and b falling in the four different regions defined in Fig. 1.

relatively large variances and high mixture fractions (mean mixture fractions greater than 0.5), Fig. 1(b).

The mass-weighted pdf is related to the unweighted pdf through [7]

$$\tilde{p}(f) = \frac{\rho}{\bar{\rho}} p(f) \tag{7}$$

The mean density is calculated as

$$\bar{\rho} = \int_0^1 \rho(f) p(f)\,\mathrm{d}f = \frac{1}{\int_0^1 \frac{1}{\rho(f)} \tilde{p}(f)\,\mathrm{d}f} \tag{8}$$

It should be pointed out that the density in the flamelet library is also dependent on the scalar dissipation rate. However, the variation of the flamelet density with the scalar dissipation rate was not taken into account in the present study since the objective of this study is to develop a robust and accurate treatment of the β-pdf integration. In addition, the integration over the scalar dissipation rate can be done efficiently using the error function as described by Lentini [4]. The density profile as a function of the mixture fraction employed in the present calculations was that obtained from a counterflow CH_4/air diffusion flame at a strain rate of 120 s^{-1} using detailed chemistry and complex transport properties. This study is therefore directly relevant to modeling turbulent diffusion combustion using fast chemistry assumptions such as the one-step irreversible reaction or the chemistry equilibrium model. The only difference is that the flamelet density profile employed in the present calculations will be slightly altered by using the one-step irreversible reaction model or the chemical equilibrium model.

Due to the approximate nature of the assumed pdf method, it is also acceptable to assume that the unweighted pdf, $p(f)$, has the form of the β-pdf given in Eq. (1) instead of the mass-weighted one, $\tilde{p}(f)$. The consequence of making this assumption will be investigated in the modeling of turbulent non-premixed combustion in a model

gas turbine combustor. In the following discussion of the numerical treatment of the β-pdf integration, it was assumed that the unweighted pdf of the mixture fraction has the β-pdf form given in Eq. (1) and the mean density is calculated as

$$\bar{\rho} = \frac{\int_0^1 \rho(f)\beta(f)\,\mathrm{d}f}{\int_0^1 \beta(f)\,\mathrm{d}f} \tag{9}$$

where

$$\beta(f) = f^{a-1}(1-f)^{b-1} \tag{10}$$

Using the property between the beta and gamma functions [8], the denominator of Eq. (9) can be written as

$$\int_0^1 f^{a-1}(1-f)^{b-1}\,\mathrm{d}f = \frac{\Gamma(a)\Gamma(b)}{\Gamma(a+b)} \tag{11}$$

The values of these gamma functions can be readily obtained by using the recurrence relation

$$\Gamma(x+1) = x\Gamma(x) \tag{12}$$

and the polynomial approximation for $0 \leqslant x \leqslant 1$ [8],

$$\Gamma(x+1) = 1 + \sum_{n=1}^{8} c_n x^n \tag{13}$$

The coefficients c's are taken from Ref. [8] and given in Table 1.

If the flamelet density distribution can be approximated by a polynomial expression of the mixture fraction, the numerator of Eq. (9) can also be easily evaluated using the beta and gamma property similar to Eq. (11). Unfortunately the flamelet density profile in general cannot be fit to a simple polynomial expression due to the steep variation of density around the reaction zone. However, it was shown by Lentini [4] that the flamelet density distribution can be fit accurately to the following expression

$$\rho(f) = \frac{\rho_{\mathrm{ref}}}{F(f)} \tag{14}$$

where ρ_{ref} is a reference density (taken as the oxidizer density ρ_{ox} in this study) and $F(f)$ is a polynomial function of the mixture fraction given as

$$F(f) = \sum_{j=0}^{J} d_j f^j \tag{15}$$

Table 1
Polynomial coefficients for calculation of the gamma function in Eq. (13)

n	c_n
1	−0.577191652
2	0.988205891
3	−0.897056937
4	0.918206857
5	−0.756704078
6	0.482199394
7	−0.193527818
8	0.035868343

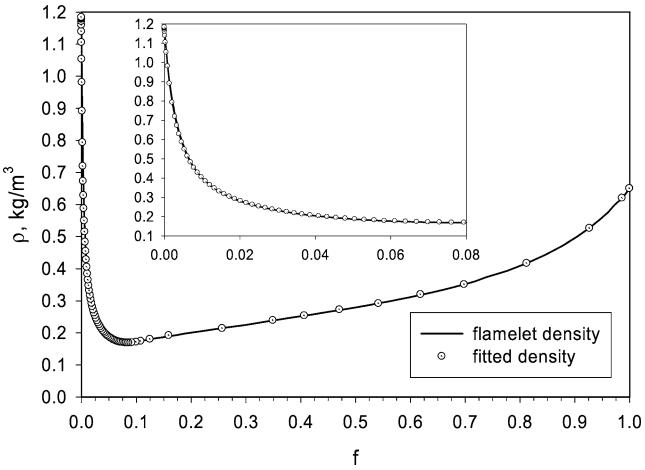

Fig. 3. Density distribution as a function of the mixture fraction calculated from a counterflow diffusion CH_4/air flame at 120 s^{-1}.

Typically the value of J is about 20 to obtain accurate fitting of Eq. (14) to the flamelet density profile. Fig. 3 shows the density distributions obtained from both the flamelet calculation of a CH_4/air flamelet at a strain rate of 120 s^{-1} and a 20-order polynomial fitted result using Eqs. (14) and (15). The fitted density distribution is in very good agreement with the density profile of the flamelet calculation.

In order to make use of the property between the beta and gamma functions, Eq. (11), given the density expression in Eq. (14), Lentini [4] apparently assumed that the mass-weighted pdf has the form of the β-pdf, though the mass-weighted pdf concept was not explicitly used in the work of Lentini. As a result, using the second part of Eq. (8), the density integration becomes

$$\bar{\rho} = \rho_{\mathrm{ref}} \frac{\int_0^1 f^{a-1}(1-f)^{b-1}\,\mathrm{d}f}{\int_0^1 F(f) f^{a-1}(1-f)^{b-1}\,\mathrm{d}f} \tag{16}$$

The denominator of Eq. (16) can now also be evaluated using the property of the beta and gamma functions as

$$\int_0^1 F(f) f^{a-1}(1-f)^{b-1}\,\mathrm{d}f = \sum_{j=0}^{J} d_j \frac{\Gamma(a+j)\Gamma(b)}{\Gamma(a+j+b)} \tag{17}$$

It is therefore advantageous to assume that mass-weighted pdf has the β-pdf form in order to make use of the relationships between beta and gamma functions given in Eqs. (11) and (17). However, these relationships cannot be used if the unweighted pdf of the mixture fraction is assumed to have the β-pdf form. In general, the semi-analytical approach of Lentini based on the properties of the beta and gamma functions cannot be used for calculations of the mean species concentrations since they cannot be fit to a polynomial expression or Eq. (14) due to their orders of magnitude variation across the reaction zone. Therefore, it is desirable to develop a general, robust, efficient and accurate numerical method for the scalar integration assuming the

β-pdf to the mixture fraction with parameters in all the four regions in the $f-g$ plane shown in Fig. 1.

The function $\beta(f)$, Eq. (10), is singular at $f=0$ if $a<1$ and singular at $f=1$ if $b<1$ as shown in Fig. 2. To remove these singularities in the numerical integration, the integration of the numerator of Eq. (9) can be divided into three parts as

$$\begin{aligned}
&\int_0^1 \rho(f) f^{a-1}(1-f)^{b-1}\,\mathrm{d}f \\
&\quad= \int_0^{\varepsilon} \rho(f) f^{a-1}(1-f)^{b-1}\,\mathrm{d}f \\
&\qquad+ \int_{\varepsilon}^{1-\varepsilon} \rho(f) f^{a-1}(1-f)^{b-1}\,\mathrm{d}f \\
&\qquad+ \int_{1-\varepsilon}^{1} \rho(f) f^{a-1}(1-f)^{b-1}\,\mathrm{d}f \\
&\quad\approx \rho_{\mathrm{ox}}\frac{\varepsilon^a}{a} + \int_{\varepsilon}^{1-\varepsilon} \rho(f) f^{a-1}(1-f)^{b-1}\,\mathrm{d}f + \rho_{\mathrm{fuel}}\frac{\varepsilon^b}{b} \qquad (18)
\end{aligned}$$

where ε is a small parameter. An effective choice for the value of ε was found to be 1.0×10^{-6} for the density calculation. A too small value of ε will increase the difficulty of the calculation of the integration in $[\varepsilon, 1-\varepsilon]$, the middle term of the right-hand side of Eq. (18). A too large value of ε will make the following approximations invalid:

(i) $(1-f)^{b-1}\approx 1$ (a good approximation for b as large as 10^4) and $\rho(f)\approx\rho_{\mathrm{ox}}$ at the oxidizer side ($f=0$), and
(ii) $f^{a-1}\approx 1$ and $\rho(f)\approx\rho_{\mathrm{fuel}}$ at the fuel side ($f=1$).

Note that these approximations were employed in deriving Eq. (18). The denominator of Eq. (9) can be calculated in a similar way to Eq. (18) as

$$\begin{aligned}
&\int_0^1 f^{a-1}(1-f)^{b-1}\,\mathrm{d}f \\
&\quad\approx \frac{\varepsilon^a}{a} + \int_{\varepsilon}^{1-\varepsilon} f^{a-1}(1-f)^{b-1}\,\mathrm{d}f + \frac{\varepsilon^b}{b} \qquad (19)
\end{aligned}$$

Using Eqs. (18) and (19) for the evaluation of the numerator and denominator therefore removes the singularity problem of the β-pdf integration. It is worth noting that Eqs. (18) and (19) are valid regardless of the values of a and b. Although both Eqs. (18) and (19) are inaccurate if $a\leqslant 1$ and b is very large (say 10^6), they still result in the correct mean density (ρ_{ox} in this case) since the second and the third terms in both equations are negligible compared to the first term in these equations. Similarly Eqs. (18) and (19) can also be used if $b\leqslant 1$ and a is very large. In situations where both a and b are greater than 1 and one or both of them are very large, a special treatment is given later to prevent overflow. Although Chen et al. [2] employed the same treatment as Eqs. (18) and (19) to remove the singularity problem for a or b or both smaller than 1, they suggested a very small value of ε (about 10^{-20}) and consequently the integration of $\beta(f)$ and $\rho(f)\beta(f)$ in domain $[\varepsilon, 1-\varepsilon]$ for a or b smaller than 1 is still difficult to calculate accurately and efficiently due to the exponential variation of this function. In addition, it is important to point out that the following two approximations derived by Chen et al. [2]

$$\bar{\rho}\approx\rho_{\mathrm{ox}}, \quad \text{if } a<1 \text{ and } a<b \qquad (20)$$

$$\bar{\rho}\approx\rho_{\mathrm{fuel}}, \quad \text{if } a>b \text{ and } b<1 \qquad (21)$$

are in general invalid unless a is very small ($\leqslant 10^{-4}$) and b is greater than 1 in Eq. (20) or b is very small and a is greater than 1 in Eq. (21).

When both a and b are greater than 1, $\beta(f)$ is no longer singular, Fig. 2, and it can be easily shown that it has a maximum that occurs at

$$f_{\max} = \frac{1}{1+(b-1)/(a-1)} \qquad (22)$$

If a or b is very large, overflow may occur. To overcome this problem, Chen et al. [2] suggested to limit the bigger value among a and b while keeping their ratio constant. For example, if a is a very large value, its value is reset to a modestly large value (say 500). The value of b is then set to,

$$b' = \frac{b}{a}a', \quad a'=500 \qquad (23)$$

where a and b are the original pdf parameters calculated from Eqs. (5) and (6). When b is very large, a and b are reset to

$$a' = \frac{a}{b}b', \quad b'=500 \qquad (24)$$

It should be pointed out that this procedure to prevent overflow problem may significantly alter the shape of the pdf determined by the original parameters a and b since the value of b' calculated from Eq. (23) or a' from Eq. (24) might be reduced from a value greater than 1 to one smaller than 1, and therefore qualitatively altering the shape of the pdf as shown in Fig. 2. A better way to prevent overflow problem while qualitatively preserving the shape of the β-pdf is to limit the bigger value of a and b while keeping the value of $f_{\max}$, i.e.,

$$b' = \frac{a'-1-f_{\max}(a'-2)}{f_{\max}}, \quad a'=500 \quad \text{if } a \text{ is very large} \qquad (25)$$

It can be shown that b' calculated from Eq. (25) is still greater than 1, therefore preserving the shape of the pdf. On the other hand, if b is very large and is to be reset, the corresponding a is then calculated as

$$a' = \frac{1 + f_{\max}(b' - 2)}{1 - f_{\max}}, \quad b' = 500 \quad \text{if } b \text{ is very large} \tag{26}$$

It can also be shown that a' is also always greater than 1. As an example, Fig. 4 shows the pdfs before and after resetting the values of a and b for $a = 3$ and $b = 2000$. It is clear from this figure that resetting the values of a and b using Eq. (26) introduces smaller distortion to the shape of the β-pdf than using Eq. (24). Therefore, to prevent the overflow problem, Eqs. (25) and (26) are preferred over Eqs. (23) and (24).

In the present treatment of the β-pdf integration the calculation of the middle terms of Eqs. (18) and (19) is carried out as follows. Only the description of the term in Eq. (18) is given to illustrate the method. It is noticed from the behavior of the function $\beta(f)$ that it varies exponentially near $f = 0$ and near $f = 1$. On the other hand, $\beta(f)$ varies rather mildly for f not too close to 0 or 1 regardless the values of a and b as shown in Fig. 5 for three pairs of a and b. The values of $\beta(f)$ for $a = 1.1$ and $b = 10$ in this figure are multiplied by 0.01 to reduce them to the magnitude of $\beta(f)$ for $a = 3$ and $b = 10$. Based on these observations, the

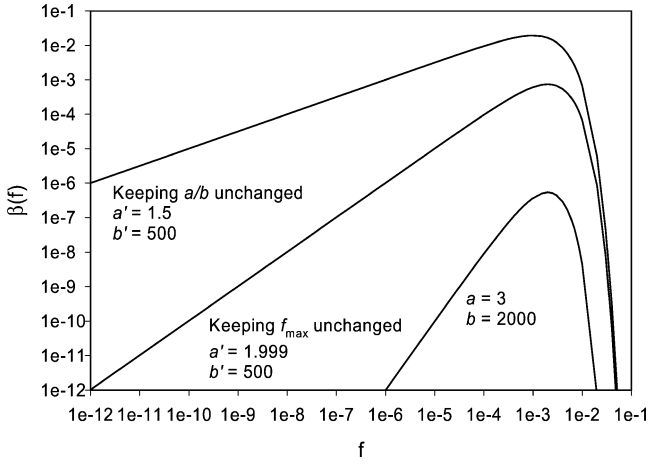

Fig. 4. Effects of resetting parameters a and b on function $\beta(f)$ using two different methods: (a) keeping the ratio a/b unchanged, and (b) keeping $f_{\max}$ unchanged.

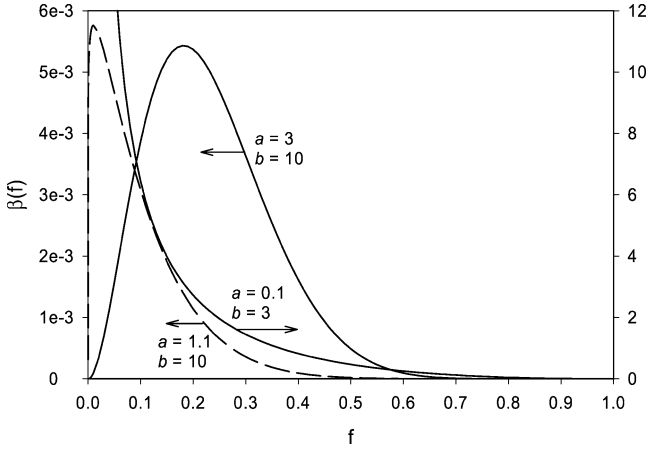

Fig. 5. Variation of $\beta(f)$ with its parameters a and b.

domain of integration is divided into several ranges whose width also varies exponentially except the range [0.1, 0.9] for the reason given above. The integration of $\rho(f)\beta(f)$ over $[\varepsilon, 1-\varepsilon]$ is therefore calculated as

$$\int_{\varepsilon}^{1-\varepsilon} \rho(f)\beta(f)\,\mathrm{d}f = \sum_{i=1}^{10} \int_{f_i}^{f_{i+1}} \rho(f)\beta(f)\,\mathrm{d}f \tag{27}$$

The values of f_i are ε, 10^{-5}, 10^{-4}, 10^{-3}, 10^{-2}, 0.1, 0.9, $1-10^{-2}$, $1-10^{-3}$, $1-10^{-4}$, $1-10^{-5}$, and $1-\varepsilon$. Integration in each sub-range is performed by simply dividing the range into N even segments, except in the range [0.1, 0.9], and the values of the function are evaluated at the center point of each segment. The range [0.1, 0.9] is divided into M even segments. To demonstrate the convergence of this algorithm for calculation over $[10^{-6}, 0.1]$ and [0.1, 0.9], Fig. 6 shows the variation of the integrated density over these two ranges with N and M for $a = 0.1$ and $b = 3.0$. It can be seen that the integrations of $\rho(f)\beta(f)$ over these two ranges converge very rapidly with increasing N and M. Similar evaluations have also been conducted for other values of a and b. It was found that $N = 20$ and $M = 50$ represent a good compromise between accuracy and efficiency for density integration and therefore these values of N and M were used in the calculations of the model gas turbine combustor. It is worth noting that larger values of N and M are in general required for the calculations

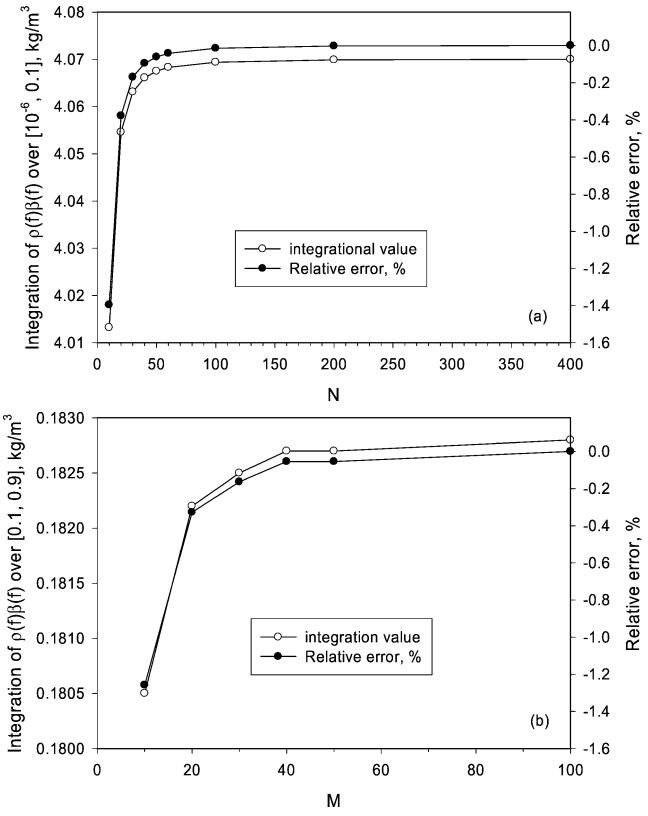

Fig. 6. Effects of N and M on the integrated density over $[1.0^{-6}, 0.1]$ and [0.1, 0.9].

of mean species concentrations due to much more drastic variation of the species concentrations with the mixture fraction than the density around the reaction zone. Use of large values of N and M in the pdf integrations of the species concentrations do not impose serious problems as far as computational efficiency is concerned since these integrations are decoupled from flow calculations.

3. Flow field calculation

The effects of turbulence on flow and combustion are accounted for using the k–ε–f–g method [9]. The governing equations solved in this method include conservation equations of mass, momentum, turbulence kinetic energy ($\tilde{k}$), dissipation rate of turbulence kinetic energy ($\tilde{\varepsilon}$), mean mixture fraction ($\tilde{f}$) and its variance ($\tilde{g}$). These equations can be written in tensor notation as

$$\frac{\partial}{\partial x_k}\left(\bar{\rho}\tilde{u}_k\right) = 0 \tag{28}$$

$$\frac{\partial}{\partial x_k}\left(\bar{\rho}\tilde{u}_k\tilde{u}_i\right) = \frac{\partial}{\partial x_k}\left[\mu_t\left(\frac{\partial \tilde{u}_i}{\partial x_k} + \frac{\partial \tilde{u}_k}{\partial x_i}\right)\right] - \frac{\partial}{\partial x_i}\left(p + \frac{2}{3}\bar{\rho}\tilde{k} + \frac{2}{3}\mu_t\frac{\partial \tilde{u}_l}{\partial x_l}\right) \tag{29}$$

$$\frac{\partial}{\partial x_k}\left(\bar{\rho}\tilde{u}_k\tilde{k}\right) = \frac{\partial}{\partial x_k}\left(\frac{\mu_t}{\sigma_k}\frac{\partial \tilde{k}}{\partial x_k}\right) + G - \bar{\rho}\tilde{\varepsilon} \tag{30}$$

$$\frac{\partial}{\partial x_k}\left(\bar{\rho}\tilde{u}_k\tilde{\varepsilon}\right) = \frac{\partial}{\partial x_k}\left(\frac{\mu_t}{\sigma_\varepsilon}\frac{\partial \tilde{\varepsilon}}{\partial x_k}\right) + C_1\frac{\tilde{\varepsilon}}{\tilde{k}}G - C_2\bar{\rho}\frac{\tilde{\varepsilon}^2}{\tilde{k}} \tag{31}$$

$$\frac{\partial}{\partial x_k}\left(\bar{\rho}\tilde{f}\right) = \frac{\partial}{\partial x_k}\left(\frac{\mu_t}{\sigma_f}\frac{\partial \tilde{f}}{\partial x_k}\right) \tag{32}$$

$$\frac{\partial}{\partial x_k}\left(\bar{\rho}\tilde{u}_k\tilde{g}\right) = \frac{\partial}{\partial x_k}\left(\frac{\mu_t}{\sigma_g}\frac{\partial \tilde{g}}{\partial x_k}\right) + C_{g_1}\mu_t\left(\frac{\partial \tilde{f}}{\partial x_k}\right)^2 - C_{g_2}\bar{\rho}\frac{\tilde{\varepsilon}}{\tilde{k}}\tilde{g} \tag{33}$$

The rate of turbulence kinetic energy production term in Eqs. (30) and (31) is given as

$$G = \mu_t\left(\frac{\partial \tilde{u}_j}{\partial x_k} + \frac{\partial \tilde{u}_k}{\partial x_j}\right)\frac{\partial \tilde{u}_j}{\partial x_k} \tag{34}$$

and $\mu_t = C_\mu\bar{\rho}\bar{k}^2/\bar{\varepsilon}$ is the turbulent eddy viscosity. Values of the model constants used in the present calculations are those commonly employed in the literature and given as $C_\mu = 0.09$, $C_1 = 1.44$, $C_2 = 1.92$, $\sigma_k = 1.0$, $\sigma_\varepsilon = 1.3$, $\sigma_f = 0.9$, $\sigma_g = 0.9$, $C_{g1} = 2.0$, and $C_{g2} = 2.0$. The standard wall function method was employed for the near wall treatment.

4. Numerical method

All the governing equations were discretized using the multi-block finite volume method described by Ferziger and Peric [10]. Convection terms were discretized using the upwind scheme while diffusion terms were discretized using the central differencing scheme. Non-staggered grid arrangement was used such that velocities and scalars, including pressure, are stored at the control volume centers. The SIMPLE algorithm was employed to handle velocity and pressure coupling [11]. The resultant algebraic equations were solved using Stone's ILU, or SIP, method [10].

5. Results and discussions

To demonstrate the efficiency, accuracy and robustness of the present numerical treatment of the β-pdf integration for mean density and flow field calculations, numerical calculations were carried out to model turbulent methane/air non-premixed combustion in a gas turbine simulator. The geometry of the combustor and various dimensions are shown in Fig. 7. The central fuel pipe radius is 4.225 mm. The inner and outer radius of the annular air port are 31.75 mm and 38.0 mm, respectively. It was assumed that the flow field in the combustor is axisymmetric. The grid used to model this axisymmetric problem is wedge shaped. Three blocks were used in the calculation. The lengths of these blocks are 42 cm, 7.675 cm, and 7.685 cm, respectively. The computational mesh used in the calculations is shown in Fig. 8. Block 1 is discretized using

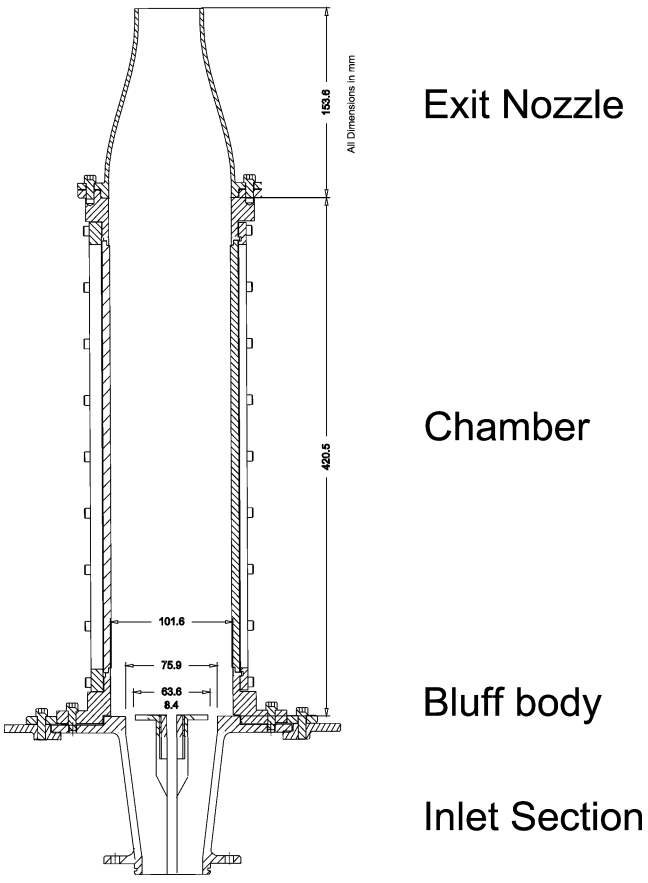

Fig. 7. Experimental setup and dimensions of the gas turbine simulator.

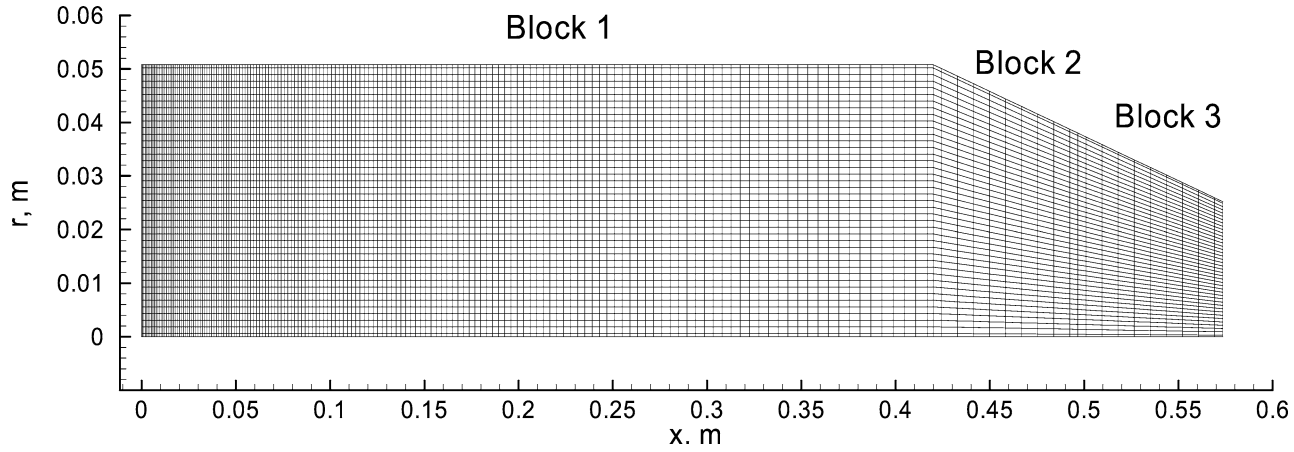

Fig. 8. Computational blocks and meshes used in the numerical calculations of the model gas turbine combustor.

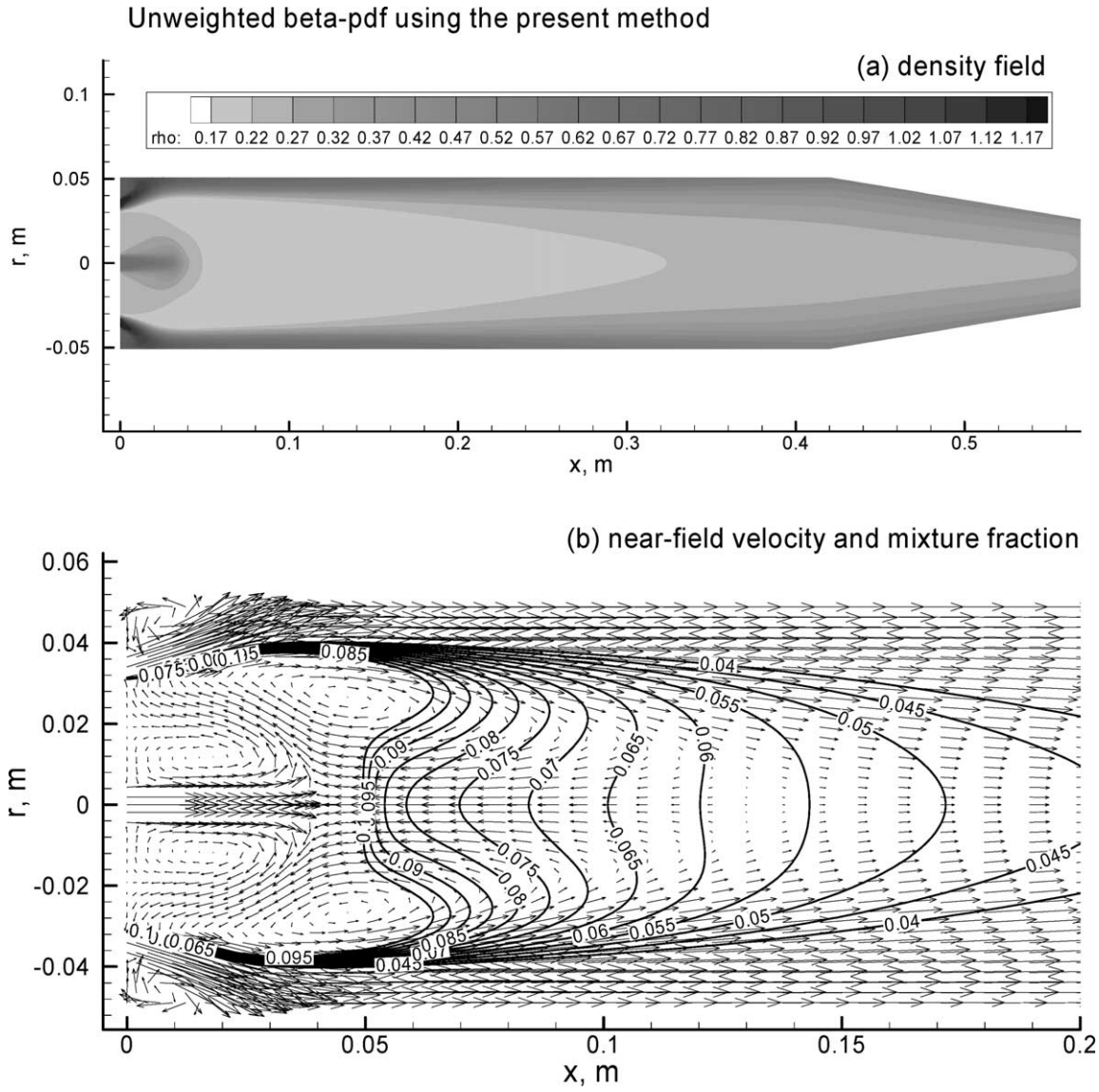

Fig. 9. Density and near-field velocity and mixture fraction distributions obtained using the present method and assuming the β-pdf to the unweighted pdf of the mixture fraction.

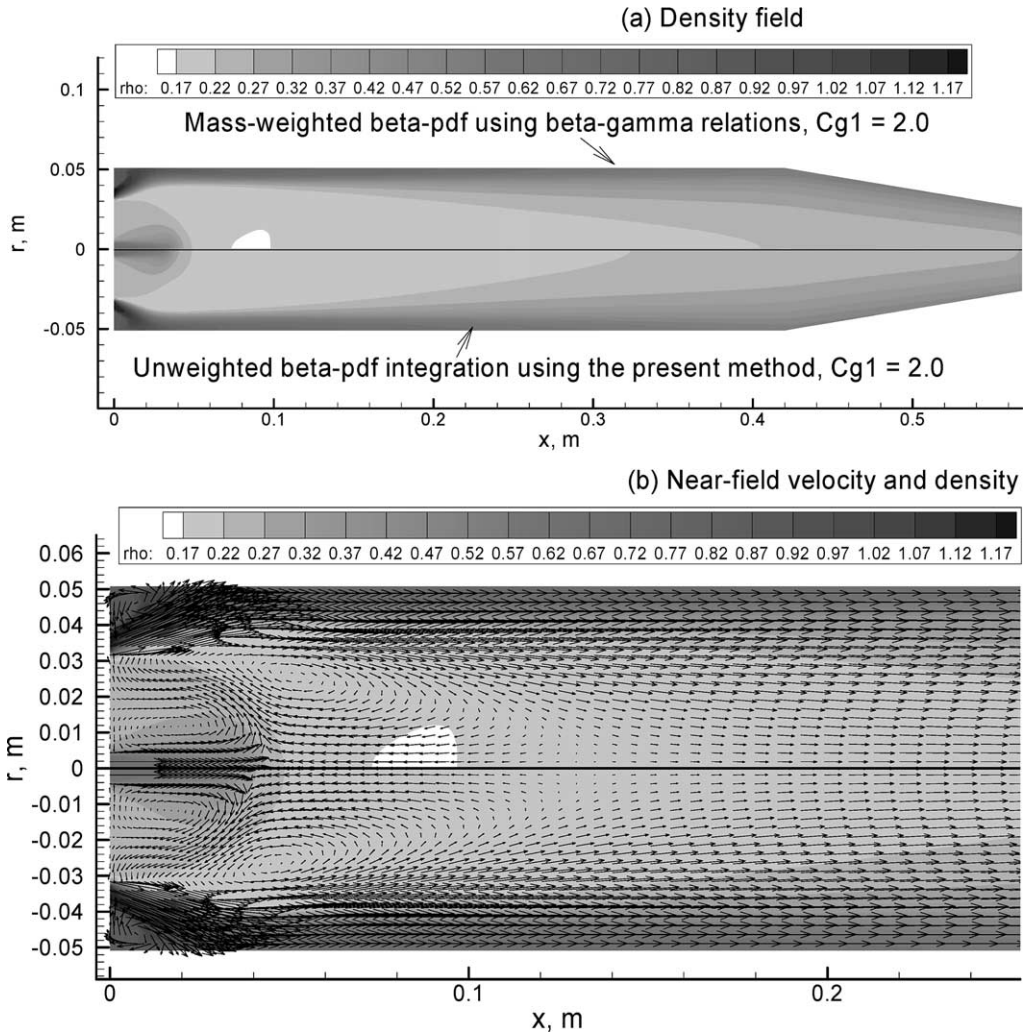

Fig. 10. Comparison of results obtained using the mass-weighted and unweighted β-pdf of the mixture fraction.

161×41 non-uniform grids with finer grids placed near the inlet region to resolve the complex flow patterns in this combustor. Blocks 2 and 3 are discretized using 9×41 grids. It has been checked that these grids are sufficiently fine to ensure grid independence of the calculated results.

Both fuel (CH_4) and air enter the combustor at 300 K. The pressure of operation is 1 atm. The inlet conditions of the fuel stream are $u = 19$ m·s^{-1}, $v = 0$, $k = 0.9$ m^2·s^{-2}, $\varepsilon = 5.5$ kg·m^{-1}·s^{-3}, $f = 1.0$, $g = 0.0$, and $\rho = 0.6517$ kg·m^{-3}. The inlet conditions for the air stream are $u = 29$ m·s^{-1}, $v = 10.5$ m·s^{-1}, $k = 1.125$ m^2·s^{-2}, $\varepsilon = 9.5$ kg·m^{-1}·s^{-3}, $f = 0$, $g = 0$, and $\rho = 1.1718$ kg·m^{-3}. Symmetry conditions are specified at the centerline of the combustor and top and bottom planes (angular direction) of the solution domain. Zero gradient conditions are imposed at the exit.

The calculated density field and the near-field distributions of velocity and the mean mixture fraction are shown in Fig. 9 assuming the unweighted β-pdf for the mixture fraction. Results displayed in the lower portion of Fig. 9 ($r < 0$) are not calculated but created using the symmetry conditions along the centerline. The flow pattern in the near field displays complex structure characterized by several recirculation zones, Fig. 9(b). The contours of the mean mixture fraction between 0.04 and 0.1 are also shown in Fig. 9(b) to indicate the mixing characteristics and the structure of the reaction zone. It is reasonable to assume that most of the chemical reactions occur in this mixture fraction range. The fuel entering the combustor through the central port first mixes with the combustion products brought back by the reverse flow around the stagnation point at $x = 0.0396$ m. The mixture of the fuel and the combustion products is then pushed outward away from the centerline and upstream by the reverse flow towards the air stream. As a result, there is a very strong mixing layer, i.e., steep gradients in the mixture fraction, right inside the annular air inlet port in the spatial region defined by $0.032 \text{ m} < r < 0.04$ m and $x < 0.06$ m. Most of the combustion takes place in this mixing layer and the centerline region between $0.05 \text{ m} < x < 0.25$ m marked by the mixture fraction contours.

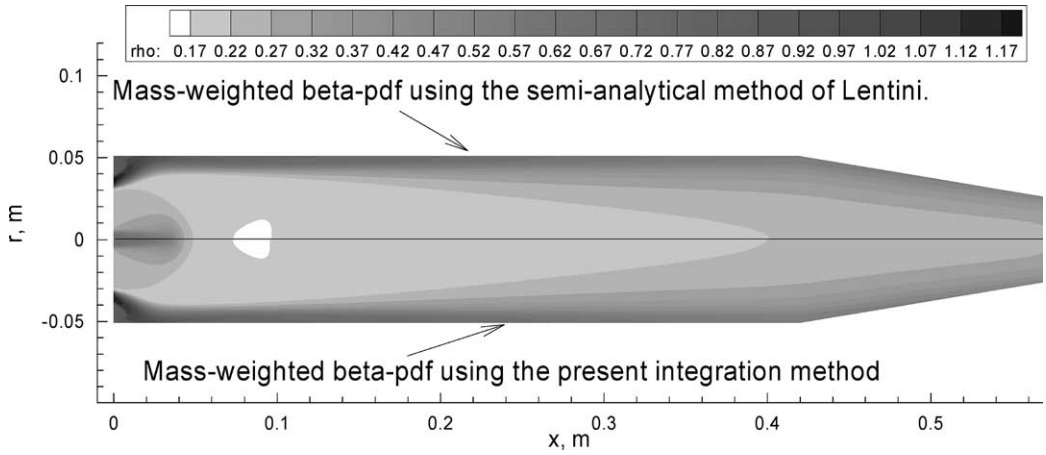

Fig. 11. Comparison of the density field calculated using the semi-analytical method of Lentini [4] and the present integration method assuming the β-pdf to the mass-weighted pdf of the mixture fraction.

Effects of assuming the β-pdf to the mass-weighted and unweighted pdf of the mixture fraction on the predictions are shown in Fig. 10 by directly comparing the two results. Although the two results are qualitatively similar, there are some quantitative differences. Applying the β-pdf to the mass-weighted pdf of the mixture fraction results in lower densities, Fig. 10(a), and the penetration of the central fuel jet is correspondingly slightly longer, Fig. 10(b), relative to that obtained using the unweighted β-pdf.

Finally Fig. 11 compares the results calculated using the semi-analytical method of Lentini [4] based on the properties of the beta and gamma functions and the present method of the β-pdf integration assuming the β-pdf to the mass-weighted pdf of the mixture fraction. The density fields calculated using these two β-pdf integration methods are in very good agreement, confirming that the present β-pdf integration method is very accurate. It was found that the β-pdf integration approach of Lentini [4] is about three times faster than the present method in the calculation of the flow field in the model gas turbine combustor. However, the present method does not suffer the limitations of the method of Lentini.

6. Conclusions

A robust and accurate numerical integration method of the β-pdf was proposed in this study. It was implemented into a 3D multiblock finite volume code to simulate turbulent CH_4/air non-premixed combustion in a model gas turbine combustor using the methodology of the flamelet model. The numerical results obtained in this study lead to the following conclusions:

(1) Assuming the β-pdf to the mass-weighted and unweighted pdfs of the mixture fraction produce quantitative differences in the calculated density and near-field velocity distributions.
(2) The calculated density field using the present β-pdf integration method is in excellent agreement with that obtained using the semi-analytical approach of Lentini.
(3) Although the present β-pdf integration method is less efficient than the method of Lentini, it is more general and does not suffer the limitations of the method of Lentini.

References

[1] N. Peters, Laminar diffusion flamelet models in non-premixed turbulent combustion, Prog. Energy Combust. Sci. 10 (1984) 319–339.
[2] C.S. Chen, K.C. Chang, J.Y. Chen, Application of a robust β-pdf treatment to analysis of thermal NO formation in nonpremixed hydrogen-air flame, Combust. Flame 98 (1994) 375–390.
[3] D. Lentini, Numerical prediction of nonpremixed turbulent flames, in: AIAA 90-0730, 28th Aerospace Sciences Meeting, Reno, Nevada, 1990.
[4] D. Lentini, Assessment of the stretched laminar flamelet approach for nonpremixed turbulent combustion, Combust. Sci. Technology 100 (1994) 95–122.
[5] D. Lentini, W.P. Jones, Numerical simulation of nonpremixed turbulent flow in a dump combustor, in: AIAA 90-1858, AIAA/SAE/ASME/ASEE 26th Joint Propulsion Conference, Orlando, FL, 1990.
[6] S. Kumar, T. Tamaru, Computation of turbulent reacting flow in a jet assisted RAM combustor, Comput. Fluids 26 (2) (1997) 117–133.
[7] K.N.C. Bray, N. Peters, Laminar flamelets in turbulent flames, in: P.A. Libby, F.A. Williams (Eds.), Turbulent Reacting Flows, Academic Press, London, 1994, pp. 80–81.
[8] P.J. Davis, Gamma function and related functions, in: M. Abramowitz, I.A. Stegun (Eds.), Handbook of Mathematical Functions, Dover, New York, 1970, pp. 255–258.
[9] A.D. Gosman, F.C. Lockwood, S.A. Syed, Prediction of a horizontal free turbulent diffusion flame, in: 16th Sympos. (Internat.) on Combustion, The Combustion Institute, 1976, pp. 1543–1555.
[10] J.H. Ferziger, M. Peric, Computational Methods for Fluid Dynamics, Springer-Verlag, Berlin, 1997, Chapters 5 and 8.
[11] S.V. Patankar, Numerical Heat Transfer and Fluid Flow, Hemisphere, Washington, DC, 1980, Chapter 7.